The Structural Mechanism for Half-the-Sites Reactivity in an Enzyme, Thymidylate Synthase, Involves a Relay of Changes between Subunits†

Amy C. Anderson,‡ Robert H. O'Neil,‡ Warren L. DeLano,§ and Robert M. Stroud*

Macromolecular Structure Group, Department of Biochemistry and Biophysics, University of California at San Francisco, San Francisco, California 94143-0448

Received July 13, 1999; Revised Manuscript Received August 23, 1999

ABSTRACT: Thymidylate synthase (TS), a half-the-sites reactive enzyme, catalyzes the final step in the de novo biosynthesis of deoxythymidine monophosphate, dTMP, required for DNA replication. The cocrystal structure of TS from *Pneumocystis carinii* (PcTS), a new drug target for an important pathogen, with its substrate, deoxyuridine monophosphate (dUMP), and a cofactor mimic, CB3717, was determined. The structure, solved at 2.6 Å resolution, shows an asymmetric dimer with two molecules of the substrate dUMP bound yet only one molecule of cofactor analogue bound. The structural evidence reveals that upon binding cofactor analogue and forming a covalent bond from the nucleophilic cysteine to the substrate, dUMP, at one active site, PcTS undergoes a conformational change that renders the opposite monomer incapable of forming a covalent bond or binding a molecule of cofactor analogue. The communication pathway between the two active sites is evident, allowing a structural definition of the basis of half-the-sites reactivity for thymidylate synthase and providing an example of such a mechanism for other half-the-sites reactive enzymes.

Thymidylate synthase (TS),[1] an obligate dimer comprised of two identical polypeptides, catalyzes the reductive methylation of deoxyuridine monophosphate (dUMP) by methylene and hydride transfer from the cofactor, 5,10-methylene tetrahydrofolate, to produce deoxythymidine monophosphate (dTMP) and dihydrofolate. TS is a half-the-sites reactive (*1*) enzyme for which binding of cofactor or an antifolate inhibitor to one monomer causes the formation of a covalent bond from the enzyme to the substrate and renders the other monomer inactive and incapable of binding cofactor. This half-the-sites reactivity has been supported by biochemical experiments showing both half-sites binding and catalytic reactions. These experiments show the same results for several different species, and it can be extrapolated that the results can be applied across species due to the strong evolutionary conservation of the biochemical and structural nature of the enzyme. Sulfhydryl titration experiments (*2*) showed that TS binds substrate and cofactor tightly in one monomer before binding in the second site. These results were confirmed by differential scanning calorimetry (*3*) and by fluorescence quenching (*4*) experiments. The fluorescence quenching experiments also determined that catalysis occurs with half-sites reactivity. Heterodimers of *Escherichia coli* TS (EcTS) with one site made inactive through mutagenesis exhibit activity equal to homodimers (*5*), further confirming catalytic half-sites reactivity. Equilibrium dialysis, gel permeation chromatography, and kinetic enzyme assays conclusively show negative cooperativity with respect to cofactor and cofactor analogue binding (*6*). Cofactor binds an enzyme/dUMP complex at one active site with a measurable dissociation constant and binds the second site so weakly that a dissociation constant cannot be calculated (*6*). Antifolate inhibitors reveal varying degrees of negative cooperativity, but the monoglutamylated versions of these inhibitors all showed between 8- and 5000-fold decreases in affinity at the second site. In summary, biochemical experiments have demonstrated that TS binds dUMP and cofactor in an ordered binding reaction in which dUMP binds one active site first followed by cofactor binding the same site and a conformational change. In the second site, dUMP binds with decreased affinity followed by cofactor binding with greatly decreased affinity. These results imply that binding reactions in one site are coupled with catalytic conversions at another site, an important and significant breakthrough in understanding the mechanism and regulation of such an essential enzyme.

The crystal structure of TS from *Pneumocystis carinii* is asymmetric with respect to binding of the cofactor mimic, the conformation of the monomers, and substrate binding. The asymmetry allows us to investigate the key signaling mechanism between the two monomers and the resultant lack of catalysis and binding of cofactor mimic at the second monomer.

EXPERIMENTAL PROCEDURES

Protein Purification, Expression, and Crystallization. P. carinii TS was expressed and purified as described previously

† Coordinates have been deposited in the PDB under accession code 1CI7.

* To whom correspondence should be addressed.

‡ These authors contributed equally to this work.

§ Present address: Sunesis Pharmaceuticals, Inc., 3696 Haven Ave., Unit C, Redwood City, CA 94063.

[1] Abbreviations: TS, thymidylate synthase; PcTS, thymidylate synthase from *Pneumocystis carinii*; dTMP, deoxythymidine monophosphate; dUMP, deoxyuridine monophosphate; EcTS, thymidylate synthase from *Escherichia coli*; DTT, dithiothreitol; FdUMP, 5-fluorodeoxyuridine monophosphate; DHFR, dihydrofolate reductase.

10.1021/bi991610i CCC: $18.00
Published on Web 10/01/1999

Table 1: Crystallographic Refinement Statistics

resolution (Å)	50−2.6
unit cell dimensions (Å)	$a = 54.05$, $b = 66.16$, $c = 178.76$
space group	$P2_12_12_1$
observed reflections	57081
unique reflections	20517
completeness (%)	81.2
R_{merge}(50−2.6 Å)	0.127
R_{factor}(50−2.6 Å)	0.216
R_{free}(50−2.6 Å)	0.293
total no. atoms	5897
no. water molecules	195
rmsd bonds (Å)	0.009
rmsd angles (deg)	1.7
average *B*-factor (Å^2)	22.2

(*7*). The protein was mixed with 2 mM dUMP, 2 mM CB3717, and 1 mM DTT and incubated on ice for 1 h. This mixture was combined in a 1:1 ratio with the crystallization solution [12.5% PEG8K, 0.2 M $(NH_4)_2SO_4$, 100 mM Tris, pH 7.5, and 1 mM DTT] in a 5 μL hanging drop and suspended over 0.75 mL of the crystallization solution. The crystals belong to space group $P2_12_12_1$ ($a = 54.05$ Å, $b = 66.16$ Å, and $c = 178.76$ Å) with one dimer per asymmetric unit.

X-ray Data Collection. Data were collected at the Stanford Synchrotron Radiation Laboratory at beamline 7-1 using crystals frozen to 100 K (30% glycerol as a cryoprotectant) and processed with the programs DENZO and SCALEPACK (*8*).

Structure Solution and Refinement. Molecular replacement procedures in AMoRe (*9*) were used to position a search model of *Cryptococcus neoformans* TS (A. Anderson, unpublished data). After the *C. neoformans* residues were replaced by *P. carinii* side chains, a $2F_o - F_c$ electron density map was calculated with the program XPLOR (*10*), and density for two molecules of the substrate, dUMP, and one molecule of the inhibitor, CB3717, was apparent, and therefore these were included in the model. Several rounds of simulated annealing using torsion angles followed by conjugate gradient minimization in CNS (*11*−*14*) and rebuilding in O (*15*) led to a final model with all residues built except three in each monomer (186−188), corresponding to a disordered loop region, and the first two N-terminal amino acids. Each residue of the molecule was verified with simulated annealing omit maps (using CNS). The final model has a crystallographic R_{factor} of 21.6% and an R_{free} of 29.3% with good geometry ($rms_{bond} = 0.009$ Å, $rms_{angle} = 1.7°$) (see refinement statistics in Table 1).

Fluorescence Spectroscopy. Measurement of the intrinsic tryptophan fluorescence was performed with a solution of 1 μM dimeric enzyme (2 μM active sites), 1 mM dUMP, and varying concentrations of CB3717 (1 nM, 5 nM, 10 nM, 50 nM, 100 nM, 500 nM, 1 μM, 5 μM, 10 μM, 50 μM, and 100 μM) in a total volume of 75 μL on an Aminco/SLM 8200 Fluorimeter. Concentrations of CB3717 greater than 100 μM absorbed significant amounts of both the excitation and emission photons from the tryptophan fluorescence and therefore were not included. The excitation wavelength was 295 nm, and emission spectra were recorded from 300 to 500 nm. The emission spectra were corrected for CB3717 fluorescence and absorption at each concentration point.

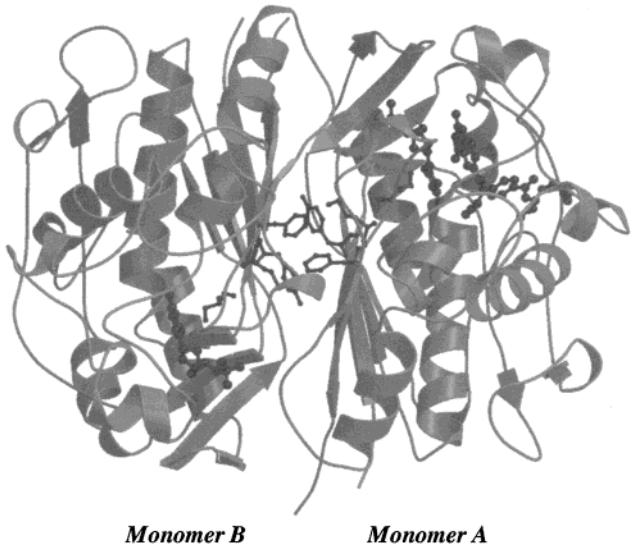

FIGURE 1: Overview of the PcTS structure with monomer A on the right-hand side and monomer B on the left. One molecule of dUMP is bound in both monomers, but only monomer A binds the cofactor analogue, CB3717 (dUMP and CB3717 shown in ball-and-stick representation). Residues involved in the signaling mechanism connecting the active sites are shown in black ball-and-stick representation and are located at the dimer interface.

RESULTS

TS from *Pneumocystis carinii* (PcTS) (Figure 1) presents the surface of an extensive central β-sheet that supports the two active sites, each site having components from both monomers. In the crystal structure, for which the dimer comprises the asymmetric unit, the substrate, dUMP, and CB3717 (N^{10}-propargyl-5,8-dideazafolic acid) are bound in the one, fully liganded active site (monomer A) in the productive configuration as seen in other species of TS (*16*−*18*). CB3717 is a strong TS inhibitor ($K_i = 90$ nM for this species of TS) (*19*), closely resembling the product, dihydrofolate. The other site, monomer B, binds only dUMP and not CB3717. Because of this unusual asymmetry, we sought an independent validation of the occupancy in each cofactor site. To assess this, the two active sites were rotated around the molecular 2-fold axis to position the two ligands from monomer A in the active site of monomer B and the one ligand from monomer B into monomer A. Thirty cycles of conjugate gradient minimization including the substituted ligands and using noncrystallographic restraints for sections of the model that do not have significantly different conformations per monomer (residues 50−130 and 147−235) were followed by calculation of a difference map (coefficients $F_o - F_c$). This 'omit-include' map shows positive density for CB3717, indicating its presence in monomer A, and negative density in monomer B, indicating that it is not present even after refinement biased by its inclusion (see Figure 2). The values of both the R_{free} and crystallographic *R*-factor for this reversed model increased (0.4% and 1.4%, respectively). The difference density reconfirms that CB3717 is bound only in monomer A and is not bound at all in monomer B. Furthermore, the active sites are not near crystal contacts. This opportunity to visualize half-the-sites binding for the antifolate is remarkable since cocrystals were grown in the presence of saturating concentrations of CB3717 (2 mM), more than 10^4 times the K_i for CB3717.

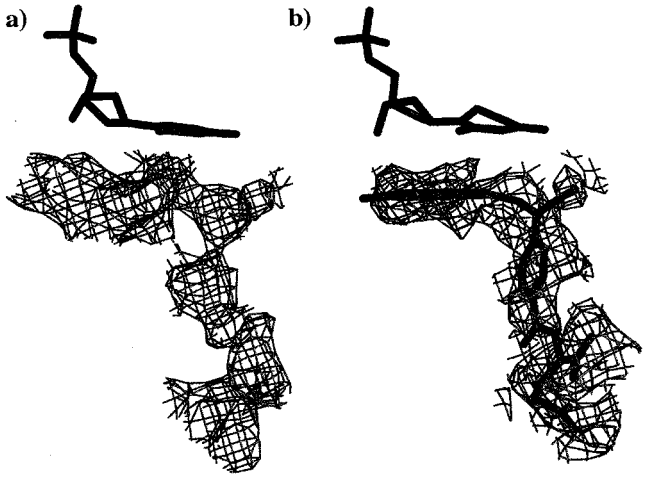

FIGURE 2: Difference electron density (shown at 1σ) for the cofactor mimic after being rotated on the molecular 2-fold axis and relocated in monomer B. (a) Positive difference electron density for the location in monomer A where the cofactor analogue is missing after relocation to monomer B. (b) Negative difference density in monomer B for the presence of the cofactor mimic.

To verify the half-sites occupancy in solution, we measured binding using the fluorescence evoked by the four tryptophan residues within each monomer. Fluorescence spectroscopy results have already shown half-sites binding in *E. coli* TS (*4*). Therefore, this method was chosen because of the strong evolutionary conservation of the enzyme and the ability to perform the experiments under the crystallization conditions. When dUMP is added to the enzyme, the intrinsic tryptophan fluorescence is reduced by 32.4%. The quenching of Trp 87 in the active site accounts for the majority of this change, as established by mutagenesis experiments in which the analogous Trp in *L. casei* TS (which contains tryptophan at all four PcTS sites) was mutated to Phe and fluorescence quenching was reduced (L. Liu, Y. Liu, and D. Santi, in preparation). As CB3717 is titrated into the enzyme in the presence of saturating concentrations of dUMP, further fluorescence quenching is accompanied by a red shift of the emission maximum from 344 to 365 nm (see Figure 3). With an enzyme concentration of 2 μM active sites, the 50% point of the fluorescence change occurs at 500 nM CB3717, indicating that the final stoichiometry is 1 CB3717 molecule per 2 active sites.

From this unique structural opportunity to visualize the inactivated site, we can begin to ask how the signal is relayed from the first liganded active site with a productive configuration to the second site where cofactor no longer binds and catalysis is inactivated. Monomer A with dUMP and the cofactor analogue CB3717 bound assumes the same "closed" productive binding interactions as in the structure of EcTS with FdUMP (*20*) and the natural cofactor. There are a total of eight hydrogen bonds (seven donors and one acceptor from the protein) to dUMP: three arginines, two from monomer B and one from monomer A, bind the phosphate and ribose of dUMP; the amide nitrogen of Asp 202 binds O2 of the pyrimidine base; Tyr 242 binds the O3′ of the ribose; and the primary specificity side chain of Asn 210 is a donor to O4 and an acceptor from 3NH of the pyrimidine. Importantly, a covalent bond is formed between the active site cysteine (Cys 173) of monomer A and the C6 position of dUMP, as would occur in the first Michael addition step of the catalytic reaction (*16*). In monomer B, there are only four hydrogen bonds to dUMP (all donors from the protein): three hydrogen bonds are from the enzyme to the phosphate, one to the O3′ of the ribose, and one to the O2 group of the pyrimidine base. These are the only hydrogen bonds that position the substrate. Importantly, Asn 210, that stabilizes the enolate intermediate in catalysis (*21*), does not form hydrogen bonds to the pyrimidine base, Tyr 242 does not form a hydrogen bond to the O3′ oxygen, and the active site cysteine in monomer B does not form a covalent bond to the substrate.

The closed conformation, triggered on binding the cofactor or its analogues, includes specific hydrogen bonds and van der Waals interactions between the active site residues and the 'closed' C-terminus and positions the substrate and cofactor for catalysis (*16*, *22*, *23*). The closed conformation allows the Michael addition reaction between the cysteine nucleophile and dUMP and initiates a cascade of conformational changes that prevent covalent bond formation and cofactor binding at monomer B. Monomer B remains in the open conformation and either lacks or exhibits weaker interactions between the active site residues and the now open C-terminus. We sought to determine the coordinated structure change between the cofactor-occupied site and monomer B by identifying residues that differ in position between monomers and are in contact along a pathway of conformational change between active sites. The results of the detailed analysis that follows are schematized in Figure 4 in which conformational changes that occur upon cofactor analogue binding in monomer A and cause the closed conformation prevent cofactor binding in monomer B.

A difference distance matrix (see Figure 5a) that compares the two monomers pinpoints regions of distinctly different conformation. The distribution of difference distances in the matrix calculation has a standard deviation of 0.25 Å, and the maximum shift is 2.47 Å. Therefore, the plots were shaded with five intervals according to a lightest value of 0.25 Å, a step size of 0.32 Å, and a darkest region corresponding to 1.87 Å. Regions of the protein including the C-terminus (residues 290−297) and loops consisting of residues 22−30, 93−98, 132−134, 204, 247−250, and 263−273 fold toward the active site when the cofactor analogue binds as indicated by the scaled vectors in Figure 5b. These conformational changes are important for the formation of both the closed ternary complex in monomer A (Figure 5c,d) and the covalent bond from the nucleophilic cysteine to the substrate. Many of these changes have been documented previously in a vector analysis comparing apo, binary (dUMP-bound), and ternary complexes of *E. coli* TS (*16*).

In addition to the global changes that occur on cofactor binding, there are subtle changes in residues at the dimer interface in a direct connection between active sites A and B. These residues are primary candidates for the signaling between active sites since the signal must go through the dimer interface and most likely involves a short and direct path. Using a least-squares superposition of monomers A and B dictated by regions of the difference distance matrix that show relatively little (<0.25 Å) change (residues 50−130 and 147−235), the shifts between the Cα atoms of monomers A and B for 34 residues that form the dimer interface were measured (see Table 2). To estimate the accuracy and reliability of the measurements of these

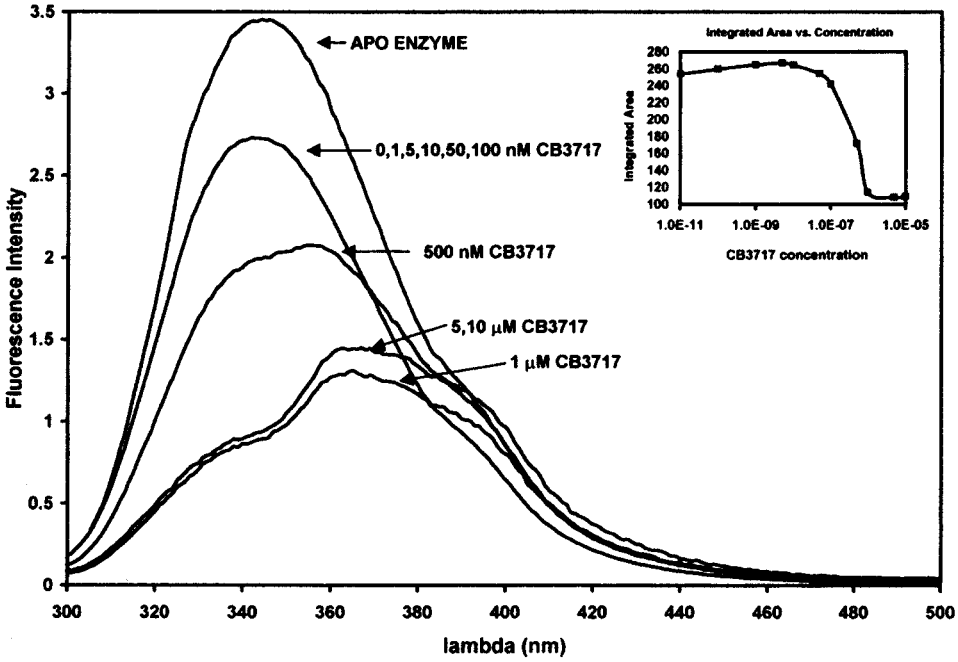

FIGURE 3: Superposition of the intrinsic tryptophan fluorescence of the enzyme alone and in the presence of saturating dUMP titrated with CB3717 during the formation of ternary complexes. CB3717 was titrated into the enzyme at concentrations of 1 nM, 5 nM, 10 nM, 50 nM, 100 nM, 500 nM, 1 μM, 5 μM, 10 μM, 50 μM, and 100 μM. The APO fluorescence shows a clear maximum at 344 nm which is quenched with the addition of dUMP at the active site. Further quenching and a shift in the maximum to 365 nm are seen with the titration of CB3717. The total area under the fluorescence curve versus the concentration of CB3717 is graphed in the inset.

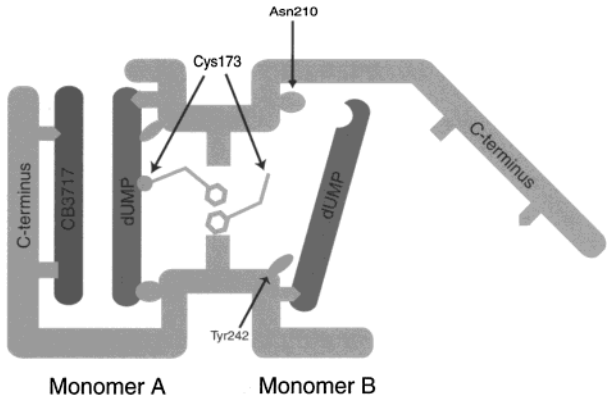

FIGURE 4: Schematic of the conformational changes PcTS undergoes on binding cofactor. When cofactor binds monomer A, the C-terminus closes the active site cavity, and Cys 173 forms a covalent bond with dUMP. These conformational changes are transferred across the dimer interface to monomer B, preventing a covalent bond. The conformational changes also result in the hydrogen bonds between Asn 210 and Tyr 242 and dUMP being broken in monomer B, yielding a misoriented dUMP and a monomer in which cofactor does not bind and catalysis is inactivated.

conformational changes, the error associated with the position of each residue was calculated using the temperature factor and atom/reflection ratio (*24*) (included in Table 2). The positions of all residues showing greater than either 0.3 Å (1.5 σ) Cα shifts or 0.4 Å (2 σ) side chain shifts are mapped to a trace of the β-sheet viewed perpendicular to the interface in Figure 6a. The majority of the dimer interface residues do not have a significant conformational change, reflecting a relatively rigid interface. However, there are several residues, specifically 173−176 and 196−199, at the dimer interface that form a direct connection between the two active sites (identified by the bound dUMP in Figure 6a) and have shifts significantly larger than the estimated error of the positions. Cys 173, the nucleophilic cysteine, shows a main chain shift of 0.35 Å and side chain shift of 0.71 Å. Met 175 has a 0.6 Å side chain shift, and Phe 176 shows both a 0.33 Å main chain and a 0.72 Å side chain shift. Residues 196 and 197 show significant main chain (0.37 and 0.35 Å, respectively) and side chain shifts, and residues 198 and 199 show large side chain shifts (0.4 and 0.54 Å). Additional singular residues exhibiting either side chain or main chain differences do not fall on this path and have no contact with the other monomers and are primarily at the ends of the strands near loop regions (residue 180), or so distant from the active site (233) that there is no obvious involvement in the passage of a signal. Although we cannot rule out other minor pathways between the active sites, the pathway through residues 173−176 and 196−199 represents the greatest structural differences between the two subunits and shows a strong coordinated movement within a rigid dimer interface and the most direct route with the most biochemical feasibility as the basis of cooperativity.

The basis for the signaling mediated by coordinated shifts of atoms in close contact between one site and the other was also addressed by the creation of a three-dimensional "movie". (W. DeLano, RigiMol, Version 1.0, under development. Information is available via the Internet at http://www.delanoscientific.com.) The movie maps an energy-minimized track between two conformational states: one an AB dimer and the other a BA dimer superposed onto the AB dimer. This structural comparison shows that the covalent Michael addition of Cys 173 to C6 of dUMP is accompanied by a 0.93 Å [error 0.2 Å (*24*)] movement of Arg 199 away from the nucleophile of Cys 173 (see Figure 7). The conformational change of Cys 173 is translated to His 174, Met 175, and Phe 176 of monomer A. Both phenylalanine residues, Phe 176 (A) in contact with Phe 176 (B), are displaced across the dimer 2-fold axis, causing the opposite

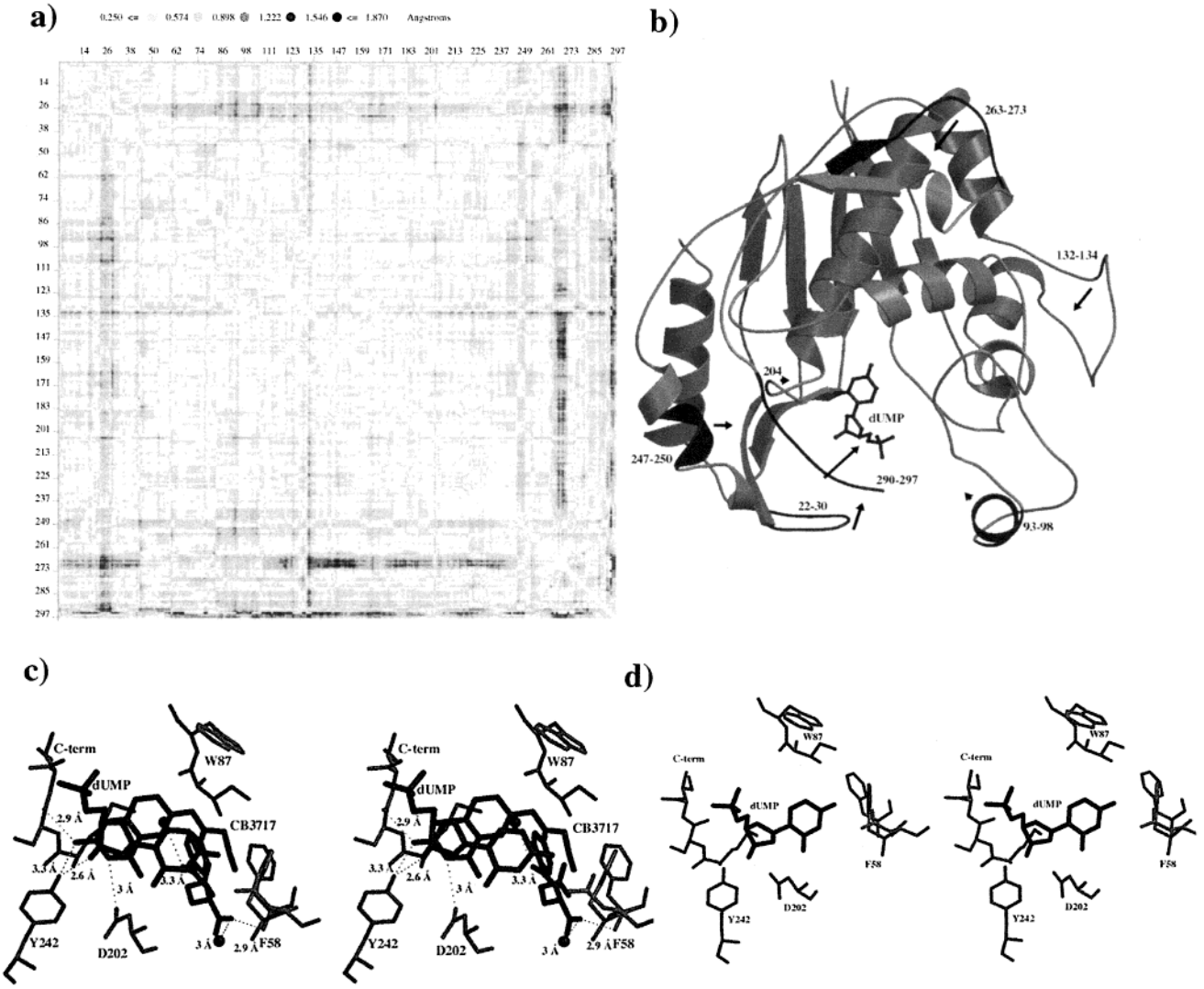

FIGURE 5: (a) Difference distance matrix comparing the conformations of monomers A and B. Residue numbers are shown on both the *x* and *y* axes. The lowest contour of the map represents one standard deviation of the plot, and five contours are shown in increasing levels. White represents a change of ≤0.25 Å; black indicates a difference of at least 1.8 Å. (b) Ribbon diagram with labeled regions corresponding to those showing the largest degree of conformational change (black). The vectors signify both the magnitude (scaled to the magnitude of the shift) and the direction of conformational change. (c) Stereoview of active site A, exhibiting the closed conformation. Distances are shown for hydrogen bonds between active site residues and the cofactor analogue. (d) Stereoview of active site B, exhibiting the open conformation.

conformational changes to occur in monomer B. As a result, the active site nucleophilic cysteine in monomer B is separated 1.58 Å further from dUMP and rotated toward Arg 199. Arg 199 is an essential side chain that polarizes Cys 173 prior to Michael addition. Additionally, the conformational changes result in the movement of two key residues, Asn 210 and Tyr 242. Asn 210 [analogous to Asn 229 in *L. casei* (*21*)] is a hydrogen bond donor to and acceptor from O2 and N3, respectively, of the pyrimidine base. The hydrogen bonds in monomer A have good geometry with lengths 2.98 and 3.4 Å, and are significantly weaker in monomer B (3.54 and 3.47 Å with poor geometry), resulting in nonproductive dUMP binding. Tyr 242 forms a hydrogen bond to the ribose 3′-oxygen in monomer A (2.6 Å) but does not form a bond in monomer B (3.5 Å) (see Figure 8). The lack of hydrogen bonds from the enzyme to the substrate in monomer B leads to a significantly misoriented substrate. From extensive mutational analysis, we have established that any misorientation of dUMP leads to an increase in the K_M for cofactor (*21*) since the cofactor is normally directly sandwiched against the pyrimidine base in a fixed orientation.

Another independent line of supporting evidence for this pathway was also obtained in PcTS. Recently we have solved the structure of PcTS bound to another antifolate inhibitor, BW1843U89 (A. Anderson, T. Surti, and R. Stroud, manuscript in preparation) to 1.9 Å resolution. This complex crystallizes in a different space group ($P2_1$) yet also reveals only one covalent bond per dimer and an asymmetry across the dimer interface residues, specifically involving Phe 176 (A) and Phe 176 (B). The occurrence of the same motifs at high resolution with a new packing arrangement reinforces the conclusions from the PcTS/dUMP/CB3717 ternary complex regarding the nature of the pathway.

DISCUSSION

The structure of PcTS is unique because usually in protein crystallography, a dimeric enzyme would appear to have 2-fold symmetry even if the two sites were slightly different, due to statistical averaging. Strict symmetry may also exist

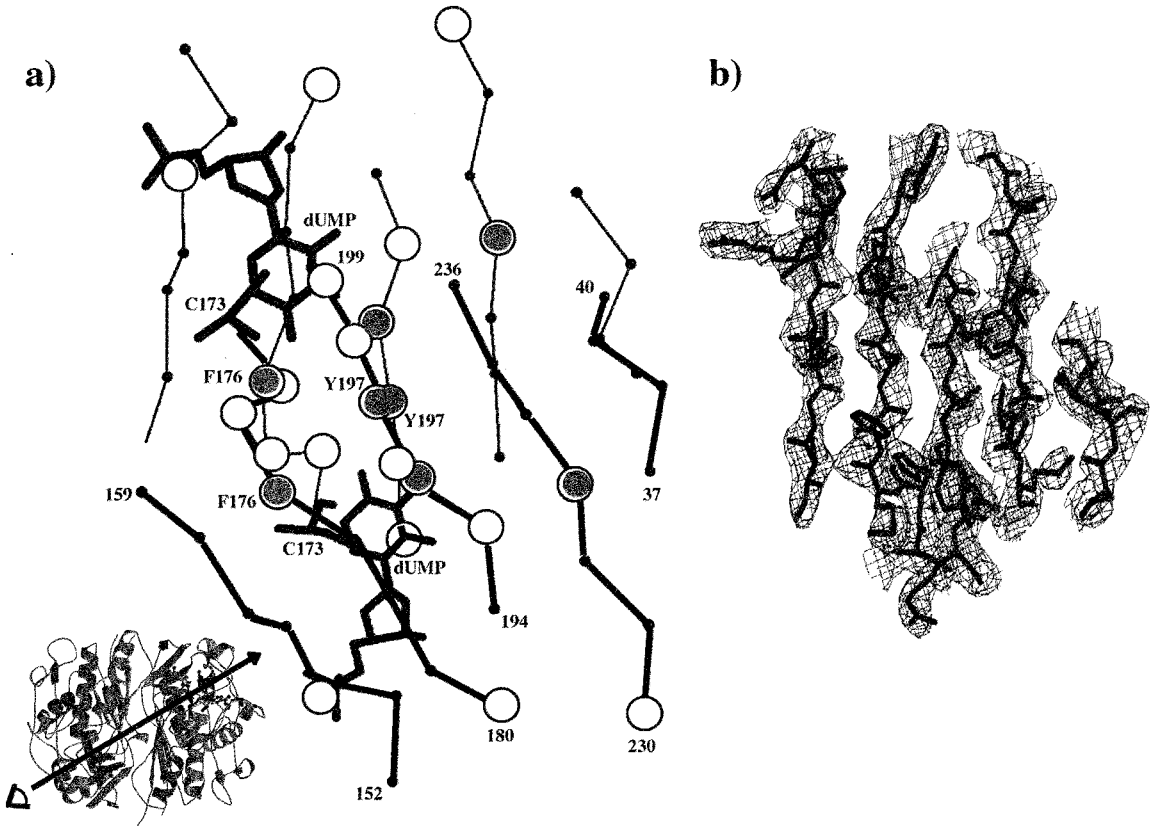

FIGURE 6: (a) Dimer interface residues with significantly different conformations in each monomer. Strands from the β-sheet of one monomer are shown in thick lines, strands from the opposite monomer are shown in thin lines, and the dUMP molecules of each active site are also shown. After superposition of the monomers using the difference distance matrix, residues with a Cα shift of greater than 0.3 Å are shown with a filled circle, and residues with a side chain movement of greater than 0.4 Å are shown with an open circle. (b) Electron density (map coefficients $2F_o - F_c$, shown at 1.3 σ) for the residues of the dimer interface.

Table 2: Residue Shifts at the Dimer Interface

residue	Cα shift (Å)	side chain shift (Å)	error (Å)[a]	residue	Cα shift (Å)	side chain shift (Å)	error (Å)
P37	0.18	0.34	0.21	**R199**	0.19	**0.54**	0.20
S38	0.18	0.19	0.23	**C173**	0.35	**0.71**	0.25
P39	0.16	0.18	0.23	H174	0.22	0.27	0.22
L40	0.16	0.13	0.20	**M175**	0.23	**0.60**	0.23
K41	0.26	0.24	0.21	**F176**	0.33	**0.72**	0.23
G230	**0.32**	0.32	0.22	C177	0.16	0.37	0.23
D231	0.22	0.31	0.21	Q178	0.15	0.28	0.21
F232	0.23	0.26	0.19	**F179**	0.21	**0.70**	0.19
I233	**0.42**	**0.42**	0.19	**Y180**	0.17	**0.49**	0.20
H234	0.26	0.25	0.19	D152	0.31	0.32	0.21
V235	0.19	0.31	0.20	R153	0.27	0.32	0.24
M236	0.23	0.21	0.21	**R154**	0.30	**0.45**	0.23
C194	0.18	0.24	0.22	L155	0.11	0.29	0.21
Q195	0.20	**0.59**	0.20	I156	0.10	0.11	0.21
L196	**0.37**	**0.38**	0.2	L157	0.14	0.18	0.20
Y197	**0.35**	0.35	0.19	S158	0.12	0.23	0.20
Q198	0.19	**0.40**	0.19	A159	0.26	0.26	0.21

[a] Error calculated using *B*-factor and atom/reflection ratio (*24*) in the following equations: slope $(B) = k_1 + k_2 * e^{(B/k_3)}$, where $k_1 = -0.687$, $k_2 = -0.00223$, and $k_3 = 6.16$; intercept $(B) = k_4 + k_5 * e^{(B/k_6)}$, where $k_4 = 0.642$, $k_5 = 0.00852$, and $k_6 = 7.88$. Error, ϵ, is then a function of *B*-factor and the atom/reflection ratio: ϵ (*B*, atom/reflection) = intercept (*B*) + slope (*B*)$*e^{(-2*\text{atom/reflection})}$. Highlighted residues show either a significant Cα or a side chain shift. Strand **1**: 37−41, **2**: 230−236, **3**: 194−199, **4**: 173−180, **5**: 152−159.

due to the coincidence of the molecular 2-fold axis with a crystallographic axis. Also, frequently the choice of saturating ligand concentrations during crystallization will fully load all sites even if the enzyme is negatively cooperative. In this particular case, however, the differences between the two monomers define a pathway of structural change that relates the bound state of monomer A to the alteration that abrogates binding at monomer B.

TS is a very highly conserved enzyme, exhibiting half-the-sites reactivity under physiological conditions throughout its evolution. With such a high degree of conservation, we might expect to see structural differences between the monomers of other species of TS. Numerous other ternary structures of TS (*16*, *20*, *25*) reveal ligand binding in both active sites and usually with some degree of asymmetry, specifically involving the phenylalanines 176 (A) and 176 (B). A comparison of the residues between the active site and the dimer interface reveals structural differences between EcTS and PcTS that may explain why EcTS can become fully loaded with ligand under saturating conditions. Important differences lie in the orientation of Phe 149 (*E. coli* numbering) and the replacement of Met 175 with Ala 148. In PcTS, the face-to-face orientation of Phe 176 from monomer A and Phe 176 from monomer B in conjunction with Tyr 197, Met 175, and Leu 196 from each monomer allows a strong coupling between monomers. In *E. coli*, Phe 149 is twisted by 126° relative to Phe 176 in PcTS, and the methionine in PcTS (Met 175) is replaced by Ala 148 with significantly less hydrophobic surface area contributed to the coupling mechanism. When one monomer in *E. coli* TS forms a covalent bond with dUMP, it demonstrates significant asymmetry but does not prohibit a covalent bond

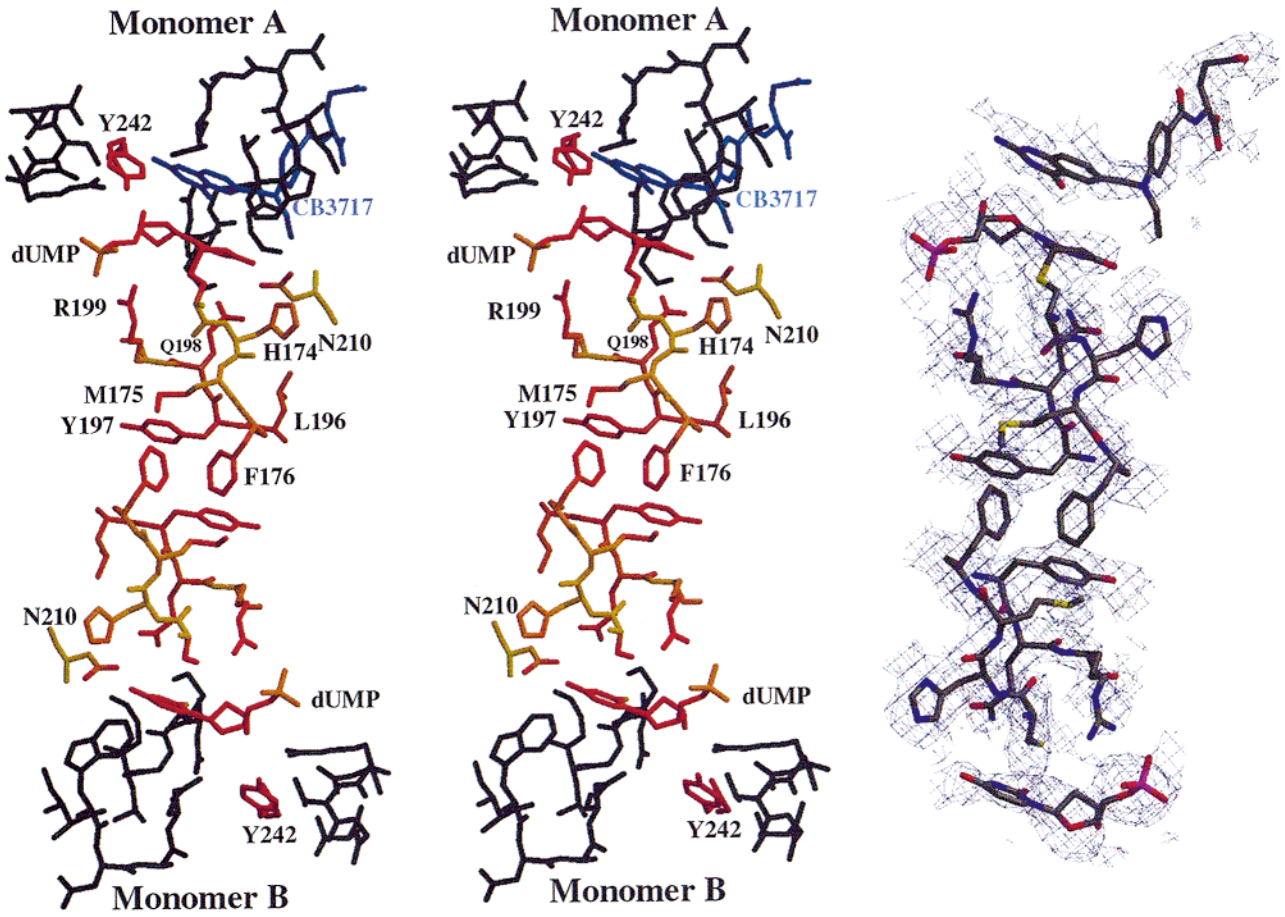

FIGURE 7: Stereoview of the residues involved in the mechanism of negative cooperativity between monomer A and monomer B. Atoms were assigned a value according to the magnitude of their shift between conformations. A color ramp was assigned (yellow to red, where red signifies the greatest shift) based on this assigned value. The cofactor mimic, CB3717, is shown in blue. Omit map electron density (shown at 1 σ) corresponding to the residues involved in the signaling mechanism is also displayed.

from forming in the opposite monomer under saturating conditions.

This structure represents a unique visualization of a direct mechanism that mediates half-the-sites reactivity in enzymology. There have been other crystal structures of negatively cooperative enzymes such as tyrosyl tRNA synthetase (*26*), D-glyceraldehyde phosphate dehydrogenase (*27*), D-amino acid aminotransferase (*28*), and indeed numerous complexes with thymidylate synthase from at least five species. However, these structures showed one monomer per asymmetric unit, a fully liganded protein (under the saturating conditions of crystal growth), or essentially identical subunits, yielding no possibility for evidence of a structural mechanism of negative cooperativity. Dihydropteroate synthase from *Staphylococcus aureus* is a half-the-sites enzyme for which the structure (*29*) shows ligand bound in only one subunit, but does not reveal any structural perturbation upon ligand binding. Additionally, the structure of adenylyltransferase from *E. coli* (*30*) reveals half-the-sites binding and significant structural differences between monomers, but a potential pathway of communication between active sites was not identified.

The aspartate receptor of *Salmonella typhimurium* exhibits strong negative cooperativity, and structures of this enzyme in the apo, singly liganded, and fully liganded forms have been solved (*31*, *32*). A serine residue at the dimer interface (*33*) as well as the relative orientation and the degree of interaction of the two monomers have been identified as important for the decreased affinity for aspartate at the second monomer. Although this receptor has a very different function from TS, it exhibits the same dependence on subtle signaling between residues at the dimer interface as well as a tight interaction between monomers.

What are the reasons for an enzyme to evolve half-the-sites reactivity? TS, one of the most highly conserved enzymes in biology, may have evolved to be a half-the-sites reactive enzyme in order to be responsive to the need for dTMP without being inhibited by two products that are structurally very similar to the substrates. With dUMP already bound at the second site, the enzyme is primed to carry out a second reaction as soon as catalysis occurs at the first site and cofactor binds the original empty site. In addition, the binding of cofactor in the opposite monomer must help products dissociate from the first monomer in a kinetically noncompetitive manner (*1*) since the dissociation constants for CB3717 are so very different at the two sites. The product, dTMP, binds TS only 3−7-fold less tightly than the substrate, dUMP, and the availability of dUMP in the cell is only 2-fold greater than dTMP (*22*). Half-the-sites reactivity can therefore give TS a regulatory advantage under physiological conditions. This proposal effectively uses the biosynthetic energy, represented by the concentrations of the fully reduced cofactor and dUMP, to help expel the products. However, there are other ways in which an enzyme could

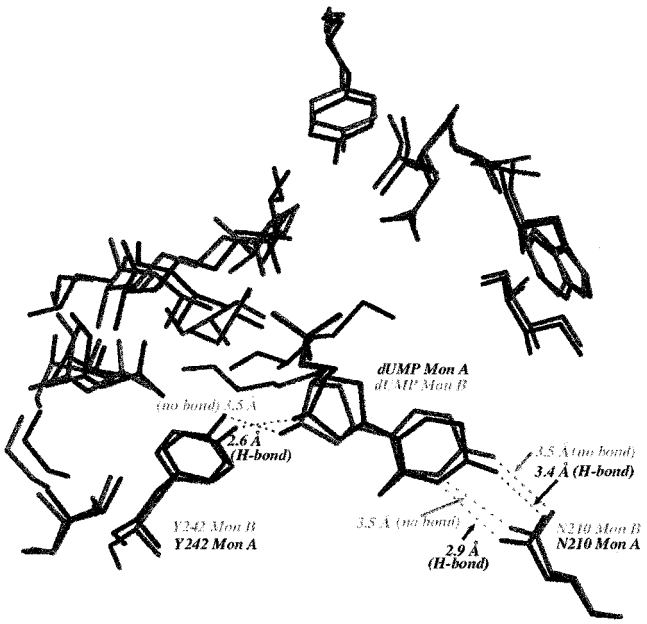

FIGURE 8: Superposition of dUMP, Asn 210, and Tyr 242 from monomers A and B. Residues from monomer A are shown in black, and those from monomer B are shown in gray. Hydrogen bonds are formed between the substrate and residues in monomer A (shown with dashed lines and distances) and are not formed in monomer B (distances are too long for hydrogen bonds).

respond to repulsion of the product. More enticing is the notion that half-the-sites reactivity is connected to the regulation of the enzyme by other enzymes with which it may be associated in the DNA replicative machinery of the cell. TS and DHFR are often found as a bifunctional protein that uses channeling to pass dihydrofolate from TS to DHFR. A cooperative involvement in the regulated pathway for folate metabolism is a very attractive prospect for how this structural mechanism could relay the state of TS activity to neighboring enzymes in the folate pathway. An assembly of such enzymes has been identified in T4 phage. This may be a fundamental aspect of biology that would not be apparent in today's in vitro assays, since it relies on the efficiency of a multienzyme pathway that is likely to be closely coupled at the structural level in the cell. These results clearly point toward a level of organization in the cell above that of TS as a soluble enzyme, and presage the notion of spatial organization of proteins in the nucleus.

ACKNOWLEDGMENT

We thank K. Perry for assistance with data collection and T. Fritz and J. Finer-Moore for discussions.

REFERENCES

1. Fersht, A., Mulvey, R., and Koch, G. (1975) *Biochemistry 14*, 13−18.
2. Danenberg, K., and Danenberg, P. (1979) *J. Biol. Chem. 254*, 4345−4348.
3. Chen, C., Davis, A., and Maley, F. (1996) *Biochemistry 35*, 8786−8793.
4. Spencer, T., Villafranca, J., and Appleman, J. (1997) *Biochemistry 36*, 4212−4222.
5. Maley, F., Pedersen-Lane, J., and Changchien, L. (1995) *Biochemistry 34*, 1469−1474.
6. Dev, I., Dallas, W., Ferone, R., Hanlon, M., McKee, D., and Yates, B. (1994) *J. Biol. Chem. 269*, 1873−1882.
7. Santi, D., Edman, U., Minkin, S., and Greene, P. (1991) *Protein Expression Purif. 2*, 350−354.
8. Otwinowski, Z. (1993) in *SERC Daresbury Laboratory*, Warrington, U.K.
9. Navaza, J. (1994) *Acta Crystallogr. A 50*, 157−163.
10. Brunger, A. (1996) *X-PLOR Version 3.8*, Yale University, New Haven, CT.
11. Brunger, A. (1992) *Nature 355*, 472.
12. Pannu, N., and Read, R. (1996) *Acta Crystallogr. A 52*, 659−668.
13. Adams, P., Pannu, N., Read, R., and Brunger, A. (1997) *Proc. Natl. Acad. Sci. U.S.A. 94*, 5018−5023.
14. Brunger, A. (1998) *Acta Crystallogr. D 54*, 905−921.
15. Jones, T., Zou, J.-Y., Cowan, S., and Kjeldgaard, M. (1991) *Acta Crystallogr. A 47*, 110−119.
16. Montfort, W., Perry, K., Fauman, E., Finer-Moore, J., Maley, G., Hardy, L., Maley, F., and Stroud, R. (1990) *Biochemistry 29*, 6964−6977.
17. Finer-Moore, J., Fauman, E., Foster, P., Perry, K., Santi, D., and Stroud, R. (1993) *J. Mol. Biol. 232*, 1101−1116.
18. Knighton, D., Kan, C., Howland, E., Janson, C., Hostomska, Z., Welsh, K., and Matthews, D. (1994) *Nat. Struct. Biol. 1*, 186−194.
19. Gangjee, A., Mavandadi, F., Kisliuk, R., McGuire, J., and Queener, S. (1996) *J. Med. Chem. 39*, 4563−4568.
20. Hyatt, D., Maley, F., and Montfort, W. (1997) *Biochemistry 36*, 4585−4594.
21. Finer-Moore, J., Liu, L., Birdsall, D., Brem, R., Apfeld, J., Santi, D., and Stroud, R. (1998) *J. Mol. Biol. 276*, 113−129.
22. Fauman, E., Rutenber, E., Maley, G., Maley, F., and Stroud, R. (1994) *Biochemistry 33*, 1502−1511.
23. Matthews, D., Appelt, K., Oatley, S., and Xuong, N. (1990) *J. Mol. Biol. 214*, 923−936.
24. Stroud, R., and Fauman, E. (1995) *Protein Sci. 4*, 2392−2404.
25. Stout, T., and Stroud, R. (1996) *Structure 4*, 67−77.
26. Brick, P., Bhat, T., and Blow, D. (1989) *J. Mol. Biol. 208*, 83−98.
27. Biesecker, G., Harris, J., Thierry, J., Walker, J., and Wonacott, A. (1977) *Nature 266*, 328−333.
28. Sugio, S., Petsko, G., Manning, J., Soda, K., and Ringe, D. (1995) *Biochemistry 34*, 9661−9669.
29. Hampele, I., D'Arcy, A., Dale, G., Kostrewa, D., Nielsen, J., Oefner, C., Page, M., Schonfeld, H., Stuber, D., and Then, R. (1997) *J. Mol. Biol. 268*, 21−30.
30. Izard, T., and Geerlof, A. (1999) *EMBO J. 18*, 2021−2030.
31. Milburn, M., Prive, G., Milligan, D., Scott, W., Yeh, J., Jancarik, J., Koshland, D., and Kim, S.-H. (1991) *Science 254*, 1342−1347.
32. Yeh, J., Biemann, H., Prive, G., Pandit, J., Koshland, D., and Kim, S.-H. (1996) *J. Mol. Biol. 262*, 186−201.
33. Kolodziej, A., Tan, T., and Koshland, D. (1996) *Biochemistry 35*, 14782−14792.

BI991610I